



**HAL**  
open science

# Modeling Channel Forms and Related Sedimentary Objects Using a Boundary Representation Based on Non-uniform Rational B-Splines

Jeremy Ruiu, Guillaume Caumon, Sophie Viseur

► **To cite this version:**

Jeremy Ruiu, Guillaume Caumon, Sophie Viseur. Modeling Channel Forms and Related Sedimentary Objects Using a Boundary Representation Based on Non-uniform Rational B-Splines. *Mathematical Geosciences*, 2016, 48 (3), pp.259-284. 10.1007/s11004-015-9629-3 . hal-01333288

**HAL Id: hal-01333288**

**<https://hal.univ-lorraine.fr/hal-01333288v1>**

Submitted on 9 Jan 2018

**HAL** is a multi-disciplinary open access archive for the deposit and dissemination of scientific research documents, whether they are published or not. The documents may come from teaching and research institutions in France or abroad, or from public or private research centers.

L'archive ouverte pluridisciplinaire **HAL**, est destinée au dépôt et à la diffusion de documents scientifiques de niveau recherche, publiés ou non, émanant des établissements d'enseignement et de recherche français ou étrangers, des laboratoires publics ou privés.

Author's revised version.

Published in *Mathematical Geosciences* 2016, 48 (3):259-284.

<http://dx.doi.org/10.1007/s11004-015-9629-3>

(c) IAMG 2015

1 **Modeling Channel Forms and Related Sedimentary Objects**  
2 **using a Boundary Representation Based on Non Uniform**  
3 **Rational B-Splines**

4 **Jeremy Ruiu, Guillaume Caumon, Sophie Viseur**

5  
6 the date of receipt and acceptance should be inserted later

7 **Abstract** In this paper, we aim at providing a flexible and compact volumetric ob-  
8 ject model capable of representing many sedimentary structures at different scales.  
9 Geo-bodies are defined by a boundary representation; each bounding surface is con-  
10 structed as a parametric deformable surface. We propose a three-dimensional sedi-  
11 mentary object with a compact parametrization which allows for representing var-  
12 ious geometries and provides a curvilinear framework for modeling internal het-  
13 erogeneities. This representation is based on Non-Uniform Rational Basis Splines  
14 (NURBS) which smoothly interpolate between a set of points. The three-dimensional  
15 models of geobodies are generated using a small number of parameters, and hence  
16 can be easily modified. This can be done by a point and click user interaction for man-  
17 ual editing or by a Monte-Carlo sampling for stochastic simulation. Each elementary  
18 shape is controlled by deformation rules and has connection constraints with associ-  
19 ated objects to maintain geometric consistency through editing. The boundary rep-  
20 resentations of the different sedimentary structures are used to construct hexahedral  
21 conformal grids in order to perform petrophysical property simulations following the  
22 particular three-dimensional parametric space of each object. Finally these properties  
23 can be upscaled, according to erosion rules, to a global grid that represents the global  
24 depositional environment.

25 **Keywords** Architectural Elements; Geobody; Surface-Based Modeling; Event-  
26 Based Modeling; Channel; Clinofolds; Meanders; Lobes

---

Jeremy Ruiu, Guillaume Caumon  
Georessources, Université de Lorraine-ENSG, CNRS, GREGU. 2 rue du Doyen Marcel Roubault F-54518  
Vandoeuvre-Lès-Nancy, France. E-mail: ruiu@gocad.org

Guillaume Caumon  
E-mail: Guillaume.Caumon@univ-lorraine.fr

Sophie Viseur  
CEREGE (UMR 7330), Aix Marseille University. 3 place Victor Hugo F-13331 Marseille cedex 03,  
France. E-mail: viseur@cerege.fr

## 1 Introduction

Most clastic deposits consist in geometric arrangements of sedimentary facies which control petrophysical heterogeneities. Capturing the spatial layout of sedimentary facies is therefore critical for subsurface modeling tasks. For instance several authors have studied the influence of small scale sedimentary heterogeneities on subsurface flow (Alpak et al, 2013; Desbarats, 1987; Haldorsen and Lake, 1984; Jackson and Muggeridge, 2000; Novakovic et al, 2002). For instance Jackson et al (2009) show that the thicknesses of sealing facies between clinoforms impact the prediction of hydrocarbon recovery volumes in shallow marine reservoirs. Jackson and Muggeridge (2000) also depict different flow behaviors depending on the scale of shale heterogeneities and the number of fluid phases. In the case of CO<sub>2</sub> storage capacity in reservoirs Issautier et al (2013) show the strong influence of heterogeneities on uncertainties related to both transport and storage capacity.

Classical approaches for facies modeling in sedimentary contexts upscale small scale core data and use geostatistical methods at the modeling grid scale to deduce spatial distribution of given properties (e.g. rock types, porosity, permeability, ...) based on their spatial probabilistic distribution. In the case of pixel-based approaches, the geometric and multi scale aspects of sedimentary heterogeneities are most commonly handled using the cookie cutter strategy (Journel, 1996; Journel et al, 1998), whereby properties are simulated within simulated facies deemed stationary. Over the past decade, multiple-point geostatistics (MPS) has emerged as an interesting practical way to describe complex channel geometries (see for instance Mariethoz and Caers (2014) and Renard and Mariethoz (2014) for reviews of recent progresses). This type of methods is based on analog training images to obtain conditional probabilities in stochastic spatial simulation processes. These approaches can be easily conditioned to dense well data. However, generating three-dimensional training images deemed representative of the geological environment remains a practical challenge in the application of MPS (Boisvert et al, 2007; Mirowski et al, 2009). In practice, object-based simulation is often used to generate training images.

Classically, object based methods (Deutsch and Wang, 1996; Deutsch and Tran, 2002; Haldorsen and Lake, 1984; Hassanpour et al, 2013; Holden et al, 1998; Shtuka et al, 1996; Viseur, 2004) simulate sedimentary bodies by sampling from probability distributions of geometric objects parameters. Internal heterogeneities are then represented in a background grid (Deutsch and Wang, 1996; Holden et al, 1998) or in a curvilinear grid defined in each channel (Shtuka et al, 1996). Object-based methods can also be applied at a smaller scale to represent centimetric to decimetric sedimentological bedforms, then upscaled to decametric scale (Wen et al, 1998; Nordahl et al, 2005).

The choice of the geometric object parametrization is non-unique and can influence the ability of the method to produce realistic sedimentary shapes. Therefore, process-oriented and pseudo-genetic methods try to model or approximate the results of depositional processes to define channel shapes (Abrahamsen et al, 2007; Howard and Knutson, 1984; Howard, 1996; Lopez, 2003; Pyrcz et al, 2009).

Most of these methods rely on grids to construct or to represent the object geometries. The limited resolution of grids can be a source of aliasing at the interfaces

72 between objects. To mitigate such approximations in object representation, several au-  
73 thors have proposed a surface-based description of object boundaries. A possible  
74 strategy consists in using the top and bottom bounding surfaces (Bertoncello et al,  
75 2013; Fisher and Wales, 1992; Graham et al, 2015; Pyrcz et al, 2005; Sech et al,  
76 2009). For instance Fisher and Wales (1992) suggest using parametric surfaces in  
77 order to capture the patterns of fluvial bodies between well data. They represent the  
78 top and bottom of the channel by two parametric surfaces yielding a boundary rep-  
79 resentation. The bounding surfaces of architectural elements can also be implicitly  
80 represented around channel axes, which makes it possible to maintain consistency of  
81 shapes during simulation and editing (Deutsch and Wang, 1996; Hassanpour et al,  
82 2013; Gai et al, 2012; Pyrcz et al, 2009).

83 This paper proposes a similar strategy using a boundary representation based on  
84 NURBS surfaces (Piegl and Tiller, 1995). The NURBS models can represent sedi-  
85 mentary bodies in many types of depositional environments, but this paper focuses  
86 on alluvial deposits (Sect. 2). As other surface-based representations, the proposed  
87 approach can accurately represent small-scale sedimentary structures without prior  
88 limitations imposed by the volumetric grid resolution. Additionally, our method di-  
89 rectly and explicitly represent volumes, in the same spirit as done by Viseur (2004)  
90 with polyhedral objects. As compared to previous methods, the proposed representa-  
91 tion makes it possible to maintain the geometric consistency of the structures during  
92 pseudo-genetic evolution. Additionally, NURBS can represent a number of 3D al-  
93 luvial features such as channel assymetry depending on meander curvature, channel  
94 bifurcation and confluence, levees, point bars and lobes (Sect. 3). Also, NURBS are  
95 compact in the sense that they can describe relatively complex geometric shapes with  
96 a limited set of parameters. In addition to CPU and RAM efficiency, this allows in-  
97 terpreters to create and deform objects with a small number of graphical interactions.  
98 This compact parameterization also makes it possible to use optimization methods  
99 to automatically reshape objects to match features in seismic or aerial images (Ruiu  
100 et al, 2015). Finally, modeling the petrophysical properties in sedimentary structures  
101 can be tedious as their distribution highly depend the geometry of the object and  
102 the support grid is not usually aligned on the heterogeneity. Managing this particu-  
103 lar distribution implies either the definition of locally varying anisotropy (Deutsch  
104 and Wang, 1996) or complex meshing approach (Shtuka et al, 1996). The volumetric  
105 representation presented in this paper allows to construct direct conformable grids  
106 for several types of architectural elements and with different types of internal archi-  
107 tectures, giving a curvilinear coordinate system for modeling internal heterogeneities  
108 (Sect. 4).

## 109 **2 Conceptual Descriptions of Sedimentary Structures**

### 110 **2.1 Alluvial Deposit Context**

111 In continental environments, rivers are the main agent of transport of sedimentary  
112 load toward coastal areas. Alluvial formations are shaped by channels which erode,  
113 transport and deposit sediments (Miall, 2010).

114 Miall (1985, 1996) decomposes river deposits in a construction of eight architec-  
115 tural elements (channels, gravelly bars and bedforms, sandy bedforms, foreset macro-  
116 forms, lateral accretion deposits, sediment gravity flow deposits, laminated sand sheets  
117 and overbank fines). These elements are equivalent in size to the channel fill, and can  
118 be differentiated by their external shape, internal geometry and facies combinations.  
119 These types of deposits are usually characterized by their good porosity and per-  
120 meability, which explain their interest in hydrocarbon exploration and production.  
121 However, owing to internal heterogeneity, alluvial reservoirs can be highly compart-  
122 mentalized (Miall, 2010).

## 123 2.2 Hierarchical Organization of Alluvial Sedimentary Structures

124 Miall (1996) describes a hierarchical classification of alluvial sedimentary structures,  
125 based on a typology of their bounding surfaces. These different structures are con-  
126 structed by multiscale nested organizations of microforms (e.g. ripple marks), meso-  
127 forms (e.g. dunes) and macroforms (e.g. point bar, levee, crevasse splay, etc) (Ta-  
128 ble 1).

129 The first order and second order bounding surfaces are microforms and meso-  
130 forms made of cross-bed surfaces with little or no internal erosion. The third order  
131 surfaces are cross-bedding erosion surfaces dipping at an angle up to  $15^\circ$ . They are  
132 usually draped with mudstones. The fourth-order surfaces are the upper bounding  
133 surface of macroforms. The fifth order surfaces limit major sand deposits such as  
134 channel fill features and channel phases. The architectural elements constituting the  
135 river deposits are of the 3<sup>rd</sup> to 5<sup>th</sup> order (Miall, 1996).

136 [Table 1 about here.]

137 Rules are defined on these bounding surfaces (Miall, 1996). A surface can truncate  
138 any surface of equal or lower order, but none of higher order. In this way, a surface  
139 always limits a set of nested bounding surfaces. Surfaces of low order can change  
140 order laterally. Bounding surfaces can disappear because of erosion. These rules can  
141 be used for the modeling of sedimentary structures using deformable templates.

## 142 3 NURBS-based Boundary Representations of Sedimentary Objects

143 We propose to construct boundary models of sedimentary structures by combining  
144 several cubic NURBS surfaces, each defined by a set of control points. These sur-  
145 faces represent an approximation of the actual body geometry. Common points be-  
146 tween surfaces must remain collocated in order to maintain the coherence of the shape  
147 throughout editing.

### 148 3.1 Mathematical Elements of NURBS

149 Non-Uniform Rational Basis Splines (NURBS) are a mathematical model commonly  
150 used in computer-aided design (CAD) for representing curves, surfaces and solids.  
151 They consist of a smooth interpolation between an ordered set of points called the

control points of the NURBS. The interpolation function is a piecewise continuous polynomial or rational function whose degree is directly related to the number of interpolated points (Piegl and Tiller, 1995). The NURBS formulation also relies on knot vectors that specify the parametric coordinates of the points separating the different interpolation functions in each direction of the parametric space. The number of elements in a knot vector is equal to the sum of the number of controls points and the degree. At a knot, the NURBS continuity is  $C^{p-k}$  where  $p$  is the degree and  $k$  is the multiplicity of the knot. Thus increasing the multiplicity of a knot creates creases in the NURBS. This feature can be used to allow for watertight connection between several smooth NURBS surfaces, for example to connect channel and levees surfaces (Sect. 3.3).

A NURBS curve  $C$  is a function of a parametric coordinate  $u$ , controlled by  $n$  control points  $P_i$  (Piegl and Tiller, 1995)

$$C(u) = \frac{\sum_{i=1}^n N_{i,p}(u)W_i P_i}{\sum_{i=1}^n N_{i,p}(u)W_i}. \quad (1)$$

Where  $p$  is the degree of the NURBS,  $W_i$  are the weights of control points and  $N_{i,p}(u)$  are the  $p^{\text{th}}$ -degree basis functions.

A NURBS surface  $S$  is defined as a tensor product of curves with two independent parameters  $(u, v)$  (Piegl and Tiller, 1995) by

$$S(u, v) = \frac{\sum_{i=1}^n \sum_{j=1}^m N_{i,p}(u)N_{j,q}(v)W_{i,j}P_{i,j}}{\sum_{i=1}^n \sum_{j=1}^m N_{i,p}(u)N_{j,q}(v)W_{i,j}}. \quad (2)$$

[Fig. 1 about here.]

Where  $p, q$  are the degrees of the NURBS in each direction of the parametric space,  $P_{i,j}$  is one control point and  $[n + 1] \times [m + 1]$  is the number of control points,  $W_{i,j}$  is the weight of the control point (Fig. 1) and  $N_{i,p}(u), N_{j,q}(v)$  are the  $p^{\text{th}}$ -degree and  $q^{\text{th}}$ -degree basis functions.

## 3.2 Channels Shapes

### 3.2.1 Description

Coarse deposit facies in alluvial environments are formed in channels. In alluvial sediments, channels are seldom observable but are deduced from paleocurrent measurement from lower-order structures (Miall, 1985). In an active channel, the sediment fill is usually sandy with coarser elements at the base of the structure (Reineck and Singh, 1980). An abandoned channel facies is more muddy due to the diminution of the sediment load (Miall, 1996). Commonly, the channel term is only used when the deposits cannot be described as lower-order sedimentary structures generated by

179 accretion processes. However, modeling channels is essential because channels con-  
180 dition the spatial layout of all other sedimentary structures in fluvial-environment. A  
181 channel geometry is usually defined by its depth, width, length and sinuosity. The top  
182 bounding surfaces can be erosional or aggradational and the bottoms are concave up  
183 erosional surfaces. Their slopes decrease when the channel width increases (Miall,  
184 1996). Channel bounding surfaces are generally from the 5<sup>th</sup> order as summarized in  
185 Table 1.

### 186 3.2.2 Construction

187 A channel form is represented by using three connected NURBS surfaces. The chan-  
188 nel shape is constructed around the backbone of the channel, which represents the  
189 line of maximum depth projected onto the top surface. The backbone is a piecewise  
190 linear curve that can be manually picked on a horizon slice or stochastically gener-  
191 ated (Deutsch and Tran, 2002; Viseur, 2004; Pyrcz et al, 2009). The 3D shape of the  
192 channel is constructed by sections which are placed at the end points of each segment  
193 of the backbone (Fig. 2). They represent the control points of the channel bounding  
194 surfaces. The shape of each channel section is defined by a width, a height and an  
195 asymmetry aspect ratio. The latter corresponds to the relative location of the back-  
196 bone between the edges of the channel, i.e. the channel section is symmetric if the  
197 asymmetry value is 0.5).

198 The top surface control net is constructed from the backbone and the width (Fig. 2(a)).  
199 In order to maintain the width of the channel each section is aligned according to the  
200 bisector of the angle formed by two consecutive segments of the backbone (Fig. 2(a)).  
201 The lateral surfaces are constructed starting from the top surface and their points are  
202 placed along a quadratic shape (Fig. 2(b)). In particular the point at the base of the  
203 quadratic function is aligned with the two above points to obtain the continuity at  
204 the channel base. A section modification process is applied to obtain an asymmet-  
205 ric shape of a channel according to its map view curvature (Fig. 2(c)). The resulting  
206 NURBS interpolation is shown on Fig. 3), which illustrates in particular the impact  
207 of channel curvature on the asymmetry (Fig. 3(b) and (c)).

208 [Fig. 2 about here.]

209 [Fig. 3 about here.]

### 210 3.2.3 Branching Channels

211 In many fluvial formations (braided, meandering, or anastomosed rivers), several  
212 channels can be connected. Avoiding geometric inconsistencies such as holes be-  
213 tween branching channels calls for special processing. The connection between two  
214 channels can be created at a section in the control mesh of the main one. The first  
215 step is to fix the backbone extremity of the branching channel, to its corresponding  
216 point on the designated section of the main channel (Fig. 4(a)).

217 The second step to connect the channel is to project the other control points of  
218 the extremity to branch onto the main channel. For an initial control point  $P$  of the

219 branching channel, the parametric coordinates of the closest point on the main chan-  
 220 nel surface is found using the Newton Method (Piegl and Tiller, 1995)

$$\begin{bmatrix} \frac{\partial}{\partial u} f(u_i, v_i) & \frac{\partial}{\partial v} f(u_i, v_i) \\ \frac{\partial}{\partial u} g(u_i, v_i) & \frac{\partial}{\partial v} g(u_i, v_i) \end{bmatrix} \cdot \begin{bmatrix} u_{i+1} - u_i \\ v_{i+1} - v_i \end{bmatrix} = \begin{bmatrix} f(u_i, v_i) \\ g(u_i, v_i) \end{bmatrix} \quad (3)$$

with  $\begin{cases} f(u_i, v_i) = \frac{\partial}{\partial u} S(u_i, v_i) \cdot (S(u_i, v_i) - P) \\ g(u_i, v_i) = \frac{\partial}{\partial v} S(u_i, v_i) \cdot (S(u_i, v_i) - P) \end{cases}$ .

221 Where are  $u_i$  and  $v_i$  the parametric coordinates at the  $i^{\text{th}}$  iteration of the projection  
 222 of  $P$  on the NURBS surface  $S(u, v)$  (side surface of the main channel on which the  
 223 branching channel is connected). The final result of the branching operation is shown  
 224 with the control net on Fig. 4(c) and without on Fig. 4(d). This process can be used  
 225 to connect either one or the two extremities of a channel. This method is used for the  
 226 manual three-dimensional interpretation (with an arbitrary depth value) of thirteen  
 227 distributary deltaic channels on a satellite image of Atchafalaya Delta near Bayou  
 228 Sale, Louisiana (Fig. 5).

229 [Fig. 4 about here.]

230 [Fig. 5 about here.]

### 231 3.2.4 Stochastic Generation

232 To stochastically generate several channels, the lines of maximum depth are sim-  
 233 ulated (Fig. 6) in a way similar to Viseur (2004): from an initial random line, lat-  
 234 eral evolution is simulated. The proposed input parameters of this generation are  
 235 the channel length, the mean amplitude of the sinuosity orthogonal to the global  
 236 stream direction  $\vec{F}$  (normalized vector), the wavelength of the sinuosity parallel to  
 237 the global channel direction and the mean width of the point bars. As noted by Abreu  
 238 et al (2003), channels can migrate both downdip along the main stream direction  $\vec{F}$   
 239 (sweep) and laterally (swing). Therefore, a growing ratio ( $\gamma$ ) corresponding to the  
 240 relative importance of both migrations is applied in the pseudo-genetic process.

241 Primarily, the growing process of the channel relies on the evaluation of tangents  
 242 and the curvatures to determine the directions and amplitudes of migration. Initializa-  
 243 tion is simply performed by an unconditional one-dimensional sequential Gaussian  
 244 simulation (Fig. 6(a)). To obtain a smooth channel trajectory, a Gaussian variogram  
 245 with is used with a range equal to half of the channel wavelength, as also done by  
 246 Deutsch and Tran (2002). Using an one-dimensional sequential Gaussian simulation  
 247 allows to obtain a relatively smooth initial channel that reproduce the mean ampli-  
 248 tude and wavelength of the channel while introducing a stochastic variability on the  
 249 initial shape. This initial variability has an impact on the final shape of the channel.  
 250 More advanced methods based on physical analogy (Pyrzcz et al, 2009), multiple-  
 251 point statistics (Mariethoz et al, 2014) or Lindenmayer systems (Rongier et al, 2015)  
 252 could also be used.

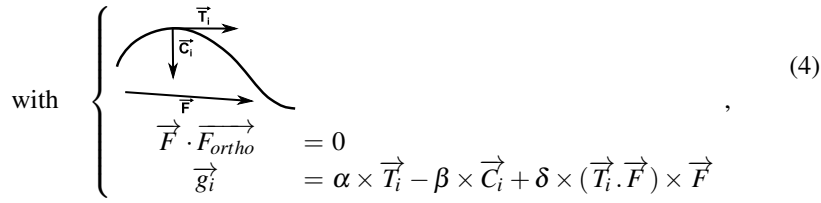
For the initial channel geometry, meandering aspects are obtained using a growing  
 process. According to Knighton (2014) the channel migration can be decomposed  
 in three elementary displacements: an extension, a translation and a rotation. In this



work, growing is obtained by displacing iteratively the control points by the following vector (Fig. 6(b))

$$\vec{G}_i = \gamma \times (\|\vec{g}_i\| \times \|\vec{F}\|) \times \vec{F} + (\|\vec{g}_i\| \times \|\vec{F}_{ortho}\|) \times \vec{F}_{ortho}$$

with  $\left\{ \begin{array}{l} \vec{F} \cdot \vec{F}_{ortho} = 0 \\ \vec{g}_i = \alpha \times \vec{T}_i - \beta \times \vec{C}_i + \delta \times (\vec{T}_i \cdot \vec{F}) \times \vec{F} \end{array} \right. , \quad (4)$



253 where  $\vec{T}_i$  is the tangent which represents the rotation component and  $\vec{C}_i$  the curvature  
 254 which represents the extension due to the lateral migration (swing (Abreu et al,  
 255 2003)).  $\vec{F}_i$  is the vector representing the global flow direction and is associated with  
 256 downdip migration of the channel (sweep (Abreu et al, 2003)). These elementary  
 257 vectors are evaluated at the projection of the control point  $i$  on the NURBS channel.  
 258 [Fig. 6 about here.]

### 259 3.3 Levees

#### 260 3.3.1 Description

261 The formation of levees is the consequence of the flooding of rivers. It results in the  
 262 deposition of a high proportion of fine sands, silts and muds organized in overlapping  
 263 lenses parallel to the channel borders. Levees consist in a sharp ridge which can reach  
 264 10 meters in thickness (Miall, 1996; Reineck and Singh, 1980). The deposits get  
 265 thinner and the facies finer as the distance from the guiding channel increases (Miall,  
 266 1996). Levee bounding surfaces are of the 4<sup>th</sup> order as summarized in Table 1.

#### 267 3.3.2 Construction

268 Levee forms are represented by using four connected NURBS surfaces. Two lateral  
 269 surfaces are used to construct the lateral faces of the levee ridge (Fig. 7(a)). The  
 270 control points are placed following a quadratic function as for channel construction.  
 271 An asymmetry aspect ratio is used to modify these surfaces in order to reproduce  
 272 the asymmetric aspect of levees (surfaces 1 and 2 on Fig. 7(b)). The third surface  
 273 represents the bottom of a levee. As levees are constructed from a guiding channel,  
 274 a fourth surface is added (surface 3 on Fig. 7(b)) to ensure the consistency in depth  
 275 between a channel and a levee. From a given channel lateral side, a levee shape is  
 276 defined by the width of the levee, the height of the levee, and an asymmetry aspect  
 277 ratio (formulated as a ratio of the width, i.e. the levee is symmetric if the value is 0.5).

278 [Fig. 7 about here.]

### 279 3.3.3 Levee-Channel Coherency

280 The coherency in depth between the channel and its levee is ensured by extracting the  
 281 portion of the common surface form between the levee and the channel down to the  
 282 appropriate depth (Fig. 8). This part of the channel side is isolated using the property  
 283 of NURBS knot vector Described in Sect. 3.1. Indeed, the multiplicity of the knot  
 284 at the desired parametric value can be increased while preserving the shape of the  
 285 NURBS (Fig. 8(b)). Thus, a knot is inserted in the appropriate channel side surface  
 286 by solving the equation (in the case of a curve) (Piegl and Tiller, 1995)

$$\sum_{i=1}^n N_{i,p}(u)P_i^W = \sum_{i=1}^{n+1} N'_{i,p}(u)Q_i^W, \quad (5)$$

287 where  $Q_i$  are the new control points and  $N'_{i,p}(u)$  are the  $p^{\text{th}}$ -degree basis functions  
 288 corresponding to the new knot vector. The equation (5) is generalized to surfaces by  
 289 applying it to each row or column of control points.

290 [Fig. 8 about here.]

291 [Fig. 9 about here.]

## 292 3.4 Lateral Accretion

### 293 3.4.1 Description

294 Lateral accretion deposits (point bars) are abundant in meandering rivers. They are  
 295 formed by the migration of a channel due to the erosional water stream outside the  
 296 bend of the channel. Point bars are formed by this continuous migration of the chan-  
 297 nel and are the result of the sediment deposition inside the bend of the channel (Rei-  
 298 neck and Singh, 1980). This type of deposit is constituted by successive clinofolds  
 299 which are macroforms delimited by third order bounding surfaces, called epsilon  
 300 cross-bedding (Allen, 1963) and constructed by the increment of lateral growth. Ep-  
 301 silon cross bedding surfaces are dipping surfaces with a dip inversely proportional  
 302 to their width/height ratio (Miall, 1985). These structures usually present a height  
 303 approximately equal to the depth of their related channel with an offlapped upper  
 304 termination and a downlapped one on the channel floor (Miall, 1996).

### 305 3.4.2 Construction

306 The clinofolds, representing the successive increments of the lateral accretion, are  
 307 constructed using six connected NURBS surfaces. Two surfaces are used to represent  
 308 the top and bottom foresets and two others for the topset and the bottomset (Fig. 10).  
 309 For the foreset, the control points are placed according to the same quadratic func-  
 310 tion as for a channel (Fig. 10(b)(c)). Two lateral surfaces are used to obtain a closed  
 311 boundary representation (Fig. 10(b)). Using this representation, the clinofold shape  
 312 is defined by the length, width and height of the clinofold, the thickness correspond-  
 313 ing to the distance between the two foresets, the amplitude of the channel which has

314 formed the clinoform and an asymmetry aspect ratio (formulated as a ratio of the  
315 width, i.e. if the value is 0.5 the clinoform is symmetric).

316 [Fig. 10 about here.]

### 317 3.4.3 Clinoform Generation from Channel Growth

318 The channels growth equation (4), can be used to generate point bars and their con-  
319 stitutive clinoforms (Fig. 11(a)). The channels of each step of the growth process  
320 intersect at the extremity of clinoforms. To determine the domain of a clinoform,  
321 the intersection between the control nets of the successive channels is computed;  
322 projecting these intersection points on the corresponding surfaces approximates the  
323 clinoform extremity locus in the parametric space (Fig. 11(b)). The portion to isolate  
324 can be determined knowing the parametric coordinates of the extremities of the cli-  
325 noforms on the original channel(Fig. 11(c)). The control points are determined using  
326 the same method as described on Fig. 8(b) to ensure the conformity between the dif-  
327 ferent clinoforms. The results and the link between the channel and its clinoforms are  
328 shown on Fig. 12.

329 [Fig. 11 about here.]

330 [Fig. 12 about here.]

331 [Fig. 13 about here.]

## 332 3.5 Crevasse Splay Lobes

### 333 3.5.1 Description

334 Lobe shapes can be present in several sedimentary deposits at different scales, such as  
335 alluvial deposits (crevasse splay), delta (deltaic lobe) and turbidite basin floor. Their  
336 usual geometry is a very large shape body (Miall, 1996; Bhattacharya, 2010; Arnott,  
337 2010). In the case of alluvial deposits this type of structure can be up to 10 km long  
338 and 5 km large. The crevasse splay sequence can be up to 10 m high and gets thinner  
339 away from the associated channel. Crevasse splay bounding surfaces are generally of  
340 4<sup>th</sup> order as summarized in Table 1.

### 341 3.5.2 Construction

342 Lobe shapes are constructed using three connected NURBS surfaces (Fig. 14). The  
343 first surface is used to construct the lobe's top. As for channels, the control points  
344 of this surface are placed along a quadratic shape. The second surface is used to  
345 construct the bottom and is flat. The third surface has the same shape as a channel  
346 section and is used to connect the lobe to its source channel (Fig. 14(c)). From a  
347 given channel object and a crevasse branching location, the lobe shape is defined by  
348 the backbone, the width and the height of the lobe.

349 [Fig. 14 about here.]

## 4 Property modeling

The sedimentary structures described in this paper provide a frame to create conformable, regular curvilinear grids. These grids define a local frame suitable to model the petrophysical properties which are controlled by depositional processes.

### 4.1 Individual Object Petrophysical Properties

#### 4.1.1 Grid Construction

The same way a NURBS surface is constructed by performing a tensor product between two NURBS curves, a NURBS volume is established using a tensor product between three curves. Considering three curves of degrees  $p$ ,  $q$  and  $r$  defined for the independent parameters  $(u, v, w)$ , a NURBS volume  $V$  is defined as

$$V(u, v, w) = \frac{\sum_{i=1}^n \sum_{j=1}^m \sum_{k=1}^l N_{i,p}(u)N_{j,q}(v)N_{k,r}(w)W_{i,j,k}P_{i,j,k}}{\sum_{i=1}^n \sum_{j=1}^m \sum_{k=1}^l N_{i,p}(u)N_{j,q}(v)N_{k,r}(w)W_{i,j,k}}, \quad (6)$$

where  $P_{i,j,k}$  is one control point and  $[n] \times [m] \times [l]$  is the number of control points,  $W_{i,j,k}$  is the weight of the control point and  $N_{i,p}(u)$ ,  $N_{j,q}(v)$ ,  $N_{k,r}(w)$  are the  $p^{\text{th}}$ -degree,  $q^{\text{th}}$ -degree and  $r^{\text{th}}$ -degree basis functions.

The three-dimensional NURBS formulation is applied to the four types of objects previously described (channels, levees, clinofolds and lobes). For each object the function is regularly evaluated in the parametric space, providing the cell corners of a hexahedral grid. If the grids are constructed from the entire parametric space they are intrinsically conformable to the bounding NURBS surfaces up to the chosen spatial resolution (Fig. 15). On the contrary if just a partition of the parametric space is taken into account (Fig. 16(c)), post-processing is required to ensure the conformity of the grid. Also, grid conformity across different objects is not necessarily guaranteed and would call for non-neighbor connections to be defined, as for instance between channel and levee (Fig. 16(d)).

[Fig. 15 about here.]

#### 4.1.2 Channel Internal Patterns

Reineck and Singh (1980), based on McKee (1957), defined three types of channel filling patterns:

- (i) By horizontal layers. This type is most common in preserved fluvial type channels.
- (ii) By concave up surfaces conforming to the channel shape. This type is usually present in submerged channels such as turbiditic ones.
- (iii) By asymmetrical inclined surfaces. This type is common in tidal influenced deposits.

379 Such internal geometries can be obtained by modifying the way the control mesh  
380 of the channel bounding surfaces is considered to construct the trivariate volumetric  
381 NURBS. For instance, the construction of the prograding grid in Fig. 16(a) is based  
382 on the mesh of the two lateral surfaces (Fig. 3). The divergent grid in Fig. 16(b) is  
383 constructed using the mesh of the top surface and by considering the two lateral sur-  
384 faces as a global bottom one. The aggrading grid Fig. 16(c) is extruded proportionally  
385 to the top surface. Then, the lower corners of the cells directly below the base surface  
386 of the channel are then vertically projected on that surface and all the underlying cells  
387 are deactivated.

388 [Fig. 16 about here.]

#### 389 4.1.3 Example of Property Modeling

390 The conformable grids of the sedimentary objects enable the easy definition of the lo-  
391 cal direction of anisotropy by performing geostatistics in the grid's parametric space.  
392 As an illustration, unconditional Sequential Gaussian Simulation is performed on  
393 grids of Fig. 16. The simulations are computed using the same variograms and the  
394 same input distributions. In this example, the effect of grid block volume variation  
395 is neglected, so more advanced simulation method could be used instead (Manchuk  
396 et al, 2005; Bertonecello et al, 2008; Manchuk and Deutsch, 2012). A realization of  
397 these simulations on each grid is presented in Fig. 17. These results illustrate the  
398 impact of the different geometries on the computation of the internal channel hetero-  
399 geneities.

400 [Fig. 17 about here.]

#### 401 4.2 Erosion between Objects and Upscaling to Reservoir grids

402 The NURBS objects presented up to now are all organized in response to the continu-  
403 ous evolution of a single channel. In reality, however, alluvial channels and associated  
404 deposits migrate laterally and vertically and can cross-cut and erode older systems. In  
405 the current state of this work, the geometries of the eroded structures are not directly  
406 computed. For each object, an uncut grid is created and filled with petrophysical  
407 properties. Erosion relations between the objects are then taken into account when  
408 transferring properties to the global reservoir grid.

409 For this, objects are ordered from their deposition order and their stratigraphic  
410 order within each deposition phase (a channel with its levees and point bars) (Table 1)  
411 (Miall, 1996). The stratigraphic order is reproduced by assigning a value to each  
412 object according to the erosive relations of their bounding surface orders defined by  
413 Miall (1996). In this case, the depth value is used to determine the deposit order of  
414 the object, assuming that the deepest objects are the oldest.

415 To illustrate the petrophysical property upscaling from the grids generated using  
416 individual geo-objects, 20 channels were stochastically generated. In the correspond-  
417 ing grids, porosity values were simulated using a Sequential Gaussian Simulation  
418 (Fig. 18(a)). The upscaling process was then performed object by object following

419 the previously defined order to reproduce the impact of erosion. The upscaling of  
 420 porosity was performed by simple volume weighted averaging (Durlafsky, 2005)

$$\phi^* = \frac{1}{V_b} \int_{V_b} \phi dV, \quad (7)$$

421 where  $\phi$  is the fine scale porosity in the fine grid over the volume  $V_b$  of coarse cell,  
 422 and  $\phi^*$  is the equivalent porosity at coarse scale. The result of this simple upscaling  
 423 process is shown on Fig. 18(b).

424 This cookie cutter strategy is not fully satisfactory because it approximates val-  
 425 ues in grid blocks crossed by the erosion surfaces. Also, thin shale drapes are not  
 426 yet taken into account in this method. More advanced and rigorous upscaling and  
 427 discretization methods should certainly be developed in the future to provide more  
 428 accurate representations of heterogeneities.

429 [Fig. 18 about here.]

## 430 5 Conclusion and discussion

431 This paper introduces a method to construct three-dimensional boundary models of  
 432 sedimentary objects and use them as a framework for petrophysical properties mod-  
 433 eling. NURBS surfaces allow the creation of boundary representations of geological  
 434 objects with great flexibility and a relatively small number of parameters (as com-  
 435 pared for instance to linear polygonal surfaces (Viseur, 2004)). This type of repre-  
 436 sentation is well adapted for modeling sedimentary structures, as interpreters can in-  
 437 teractively fit these surfaces to data. A priori knowledge about the three-dimensional  
 438 shape of the sedimentary structures can be maintained because derivative and cur-  
 439 vature constraints can be defined. To create boundary representation of sedimentary  
 440 structures, a control point hierarchy has to be created in order to keep the connection  
 441 of common points between faces.

442 Pseudo-genetic lateral migration has been proposed to automatically generate point  
 443 bar structures from channel migration. This process can be inverted to help point bar  
 444 reconstruction from observed channels (Ruiu et al, 2015). As presented in Appendix  
 445 A, further refinement can be introduced in the forward channel migration process to  
 446 generate oxbow lakes. These geobodies could easily be populated by abandonment  
 447 shale facies. Currently, the proposed method only deals with lateral migration and  
 448 does not include stacking patterns due to vertical aggradation and avulsion. The main  
 449 limitation to deal with these processes lies in the extraction of point bars during the  
 450 channel growth as it relies on the intersections between the channel's top surfaces  
 451 control nets, which is not applicable in case of channel vertical migration. A possible  
 452 enhancement could be to more generally compute intersections between all consti-  
 453 tuting surfaces of the successive channels.

454 Concerning the property modeling, the gridding of the objects allows the model-  
 455 ing of the internal heterogeneities in the sedimentary structures and to transfer them  
 456 in a background grid. Heterogeneities at the interfaces between objects (e.g. shale  
 457 lens deposits between clinoforms in point bars) are not yet considered. This could be  
 458 simulated in the parametric spaces of the sedimentary structure boundary surfaces as

done by Li and Caers (2011) and integrated in the reservoir grid as transmissibility multipliers.

In this work, only deterministic values are considered for the parameter used to construct the different objects. It would be interesting to simulate these parameters to generate more diverse shapes, to be used for instance as input training images in multi-point simulation. Future work also includes the definition of architectural element templates adapted to other depositional environments (turbiditic, deltaic, ...).

In subsurface applications involving the presence of conditioning data, two main avenues can be considered to use the proposed object models. The simplest strategy is to generate non-conditional realizations to be then used as training images for multiple-point geostatistical simulation (Comunian et al, 2014). Alternatively, significant research should still be done to allow for data conditioning directly on the proposed object models (Viseur, 2004; Pyrcz et al, 2009; Bertonecello et al, 2008; Ruiu et al, 2015).

## 6 Acknowledgements

This research was performed in the frame of the Research for Integrative Numerical Geology (RING) project. We would like to thank our colleagues from RING for their help during the development of the project. The companies and universities members of the GOCAD consortium managed by ASGA (<http://www.ring-team.org/index.php/consortium/>) are acknowledged for their support. We thank Paradigm for providing the SKUA-GOCAD software and development kit.

## References

- Abrahamsen P, Fjellvoll B, Hauge R (2007) Process based stochastic modelling of deep marine reservoirs. In: EAGE Petroleum Geostatistics
- Abreu V, Sullivan M, Pirmez C, Mohrig D (2003) Lateral accretion packages (laps): an important reservoir element in deep water sinuous channels. *Marine and Petroleum Geology* 20(6):631–648
- Allen JR (1963) The classification of cross-stratified units. with notes on their origin. *Sedimentology* 2(2):93–114
- Alpak FO, Barton MD, Naruk SJ (2013) The impact of fine-scale turbidite channel architecture on deep-water reservoir performance. *AAPG Bull* 97(2):251–284, DOI 10.1306/04021211067
- Arnott R (2010) Deep-marine sediments and sedimentary systems. In: James N, Dalrymple R (eds) *Facies Model 4*, St. John's: Geological Association of Canada, pp 295–322
- Bertonecello A, Caers JK, Biver P, Caumon G (2008) Geostatistics on stratigraphic grids. In: Ortiz J, Emery X (eds) *Proc. eighth Geostatistical Geostatistics Congress*, Gecamin ltd, vol 2, pp 677–686
- Bertonecello A, Sun T, Li H, Mariethoz G, Caers J (2013) Conditioning surface-based geological models to well and thickness data. *Math Geosci* 45(7):873–893

- 499 Bhattacharya J (2010) Deltas. In: James N, Dalrymple R (eds) *Facies Model 4*,  
500 St. John's: Geological Association of Canada, pp 233–264
- 501 Boisvert JB, Pycrz MJ, Deutsch CV (2007) Multiple-point statistics for training im-  
502 age selection. *Nat Resour Res* 16(4):313–321
- 503 Comunian A, Jha SK, Giambastiani BM, Mariethoz G, Kelly BF (2014) Training im-  
504 ages from process-imitating methods. *Mathematical Geosciences* 46(2):241–260
- 505 Desbarats A (1987) Numerical estimation of effective permeability in sand-shale for-  
506 mations. *Water Resour Res* 23(2):273–286
- 507 Deutsch C, Tran T (2002) Fluvsim: a program for object-based stochastic modeling  
508 of fluvial depositional systems. *Comput Geosci* 28(4):525–535
- 509 Deutsch CV, Wang L (1996) Hierarchical object-based stochastic modeling of fluvial  
510 reservoirs. *Math Geol* 28(7):857–880
- 511 Durlofsky LJ (2005) Upscaling and gridding of fine scale geological models for flow  
512 simulation. In: 8th International Forum on Reservoir Simulation, Borromees Is-  
513 land, Stresa, Italy, pp 20–24
- 514 Fisher T, Wales R (1992) Rational splines and multidimensional geologic modeling.  
515 In: Pflug R, Harbaugh J (eds) *Computer Graphics in Geology*, Lecture Notes in  
516 Earth Sciences, vol 41, Springer Berlin / Heidelberg, pp 17–28
- 517 Gai X, Wu Xh, Branets L, Sementelli K, Robertson G (2012) Concept-based geo-  
518 logic modeling using function form representation. In: Abu Dhabi International  
519 Petroleum Conference and Exhibition
- 520 Google Earth (October, 29 2012) Atchafalaya delta 29°30'02.17"N 91°25'50.54"O
- 521 Graham GH, Jackson MD, Hampson GJ (2015) Three-dimensional modeling of cli-  
522 noforms in shallow-marine reservoirs: Part 1. Concepts and application. *AAPG*  
523 *Bulletin* 99(06):1013–1047, DOI 10.1306/01191513190
- 524 Haldorsen H, Lake L (1984) A new approach to shale management in field-scale  
525 models. *Old SPE J* 24(4):447–457
- 526 Hassanpour MM, Pycrz MJ, Deutsch CV (2013) Improved geostatistical models of  
527 inclined heterolithic strata for McMurray formation, Alberta, Canada. *AAPG Bull*  
528 97(7):1209–1224, DOI 10.1306/01021312054
- 529 Holden L, Hauge R, Skare Ø, Skorstad A (1998) Modeling of fluvial reservoirs with  
530 object models. *Math Geol* 30(5):473–496
- 531 Howard A (1996) Modelling channel evolution and floodplain morphology. *Flood-*  
532 *plain processes* pp 15–62
- 533 Howard A, Knutson T (1984) Sufficient conditions for river meandering: A simula-  
534 tion approach. *Wat Resour Res* 20(11):1659–1667
- 535 Issautier B, Fillacier S, Gallo YL, Audigane P, Chiaberge C, Viseur S (2013) Mod-  
536 elling of CO<sub>2</sub> injection in fluvial sedimentary heterogeneous reservoirs to assess  
537 the impact of geological heterogeneities on CO<sub>2</sub> storage capacity and performance.  
538 *Energy Procedia* 37(0):5181 – 5190
- 539 Jackson M, Muggeridge A (2000) Effect of discontinuous shales on reservoir perfor-  
540 mance during horizontal waterflooding. *SPE J* 5(4):446–455
- 541 Jackson MD, Hampson GJ, Sech RP (2009) Three-dimensional modeling of a  
542 shoreface-shelf parasequence reservoir analog: Part 2. geologic controls on fluid  
543 flow and hydrocarbon recovery. *AAPG Bull* 93(9):1183–1208, DOI 10.1306/  
544 05110908145



- 545 Journal A (1996) Conditional simulation of geologically averaged block permeabili-  
546 ties. *J hyd* 183(1):23–35
- 547 Journal A, Gunderso R, Gringarten E, Yao T (1998) Stochastic modelling of a fluvial  
548 reservoir: a comparative review of algorithms. *J Pet Sci and Eng* 21(1):95–121
- 549 Knighton D (2014) *Fluvial forms and processes: a new perspective*, 2nd edn. Rout-  
550 ledge, New York, NY.
- 551 Li H, Caers J (2011) Geological modelling and history matching of multi-scale flow  
552 barriers in channelized reservoirs: methodology and application. *Petrol Geosci*  
553 17(1):17–34, DOI 10.1144/1354-079309-825
- 554 Lopez S (2003) *Modélisation de réservoirs chenalisés méandriformes: une approche*  
555 *génétique et stochastique*. PhD thesis, Mines Paris Tech
- 556 Manchuk J, Leuangthong O, Deutsch CV (2005) Direct geostatistical simulation on  
557 unstructured grids. In: *Geostatistics Banff 2004*, Springer, pp 85–94
- 558 Manchuk JG, Deutsch CV (2012) Implementation aspects of sequential gaussian sim-  
559 ulation on irregular points. *Computational Geosciences* 16(3):625–637
- 560 Mariethoz G, Caers J (2014) *Multiple-point Geostatistics: Stochastic Modeling with*  
561 *Training Images*. Wiley-Blackwell
- 562 Mariethoz G, Comunian A, Irazzaval I, Renard P (2014) Analog-based meandering  
563 channel simulation: ANALOG-BASED MEANDERING CHANNEL SIMULA-  
564 TION. *Water Resources Research* 50(2):836–854, DOI 10.1002/2013WR013730
- 565 McKee ED (1957) Flume experiments on the production of strati-  
566 fication and cross-stratification. *J Sed Res* 27(2):129–134, DOI  
567 10.1306/74D70678-2B21-11D7-8648000102C1865D
- 568 Miall A (1985) Architectural-element analysis: a new method of facies analysis ap-  
569 plied to fluvial deposits. *Earth-Sci Rev* 22(4):261–308
- 570 Miall A (1996) *Geology of Fluvial Deposits: Sedimentary Facies*. Springer Verlag
- 571 Miall A (2010) Alluvial deposits. In: James N, Dalrymple R (eds) *Facies Model 4*,  
572 St.John's:Geological Association of Canada, pp 105–138
- 573 Mirowski PW, Tetzlaff DM, Davies RC, McCormick DS, Williams N, Signer C  
574 (2009) Stationarity scores on training images for multipoint geostatistics. *Math*  
575 *Geosci* 41(4):447–474
- 576 Nordahl K, Ringrose PS, Wen R (2005) Petrophysical characterization of a het-  
577 erolithic tidal reservoir interval using a process-based modelling tool. *Petrol*  
578 *Geosci* 11(1):17–28
- 579 Novakovic D, White C, Corbeanu R, Hammon Iii W, Bhattacharya J, McMechan G  
580 (2002) Hydraulic effects of shales in fluvial-deltaic deposits: Ground-penetrating  
581 radar, outcrop observations, geostatistics, and three-dimensional flow modeling for  
582 the Ferron sandstone, Utah. *Math Geol* 34(7):857–893
- 583 Piegl L, Tiller W (1995) *The NURBS book*. Springer-Verlag, London, UK
- 584 Pycrz M, Boisvert J, Deutsch C (2009) Alluvsim: A program for event-based stochas-  
585 tic modeling of fluvial depositional systems. *Comput Geosci* 35(8):1671 – 1685,  
586 DOI 10.1016/j.cageo.2008.09.012
- 587 Pycrz MJ, Catuneanu O, Deutsch CV (2005) Stochastic surface-based modeling of  
588 turbidite lobes. *AAPG Bulletin* 89(2):177–191, DOI 10.1306/09220403112
- 589 Reineck HE, Singh IB (1980) *Depositional Sedimentary Environments*. Springer,  
590 Berlin-Heidelberg

- 591 Renard P, Mariethoz G (2014) Special issue on 20 years of multiple-point statistics:  
592 Part 1. *Math Geosci* 46(2):129–131
- 593 Rongier G, Collon P, Renard P, Ruiu J (2015) Channel simulation using L-system,  
594 potential fields and NURBS. In: *Petroleum Geostatistics 2015*, EAGE, DOI 10.  
595 3997/2214-4609.201413604
- 596 Ruiu J, Caumon G, Viseur S, Antoine C (2014) Modeling channel forms using a  
597 boundary representation based on non-uniform rational b-splines. In: *Mathematics*  
598 *of Planet Earth*, Springer, pp 581–584
- 599 Ruiu J, Caumon G, Viseur S (2015) Semiautomatic interpretation of 3d sedimento-  
600 logical structures on geologic images: An object-based approach. *Interpretation*  
601 3(3):SX63–SX74
- 602 Sech RP, Jackson MD, Hampson GJ (2009) Three-dimensional modeling of a  
603 shoreface-shelf parasequence reservoir analog: Part 1. surface-based modeling to  
604 capture high-resolution facies architecture. *AAPG Bulletin* 93(9):1155–1181, DOI  
605 10.1306/05110908144
- 606 Shtuka A, Samson P, Mallet JL (1996) Petrophysical simulation within an object-  
607 based reservoir model. In: *Proc. European 3D Reservoir Modelling Conference*  
608 (SPE 35480)
- 609 Viseur S (2004) Turbidite reservoir characterization : object-based stochastic simula-  
610 tion meandering channels. *B Soc Geol Fr* 175(1):11–20, DOI 10.2113/175.1.11
- 611 Wen R, Martinius A, Næss A, Ringrose P (1998) Three-dimensional simulation of  
612 small-scale heterogeneity in tidal deposits—a process-based stochastic simulation  
613 method. In: ) *Proceedings of the 4th Annual Conference of the International Asso-*  
614 *ciation of Mathematical Geology (IAMG)*. De Frede editore, Ischia, pp 129–134

## 615 Appendix A: Construction of an oxbow lake

616 Oxbow lakes are formed during the lateral migration of a channel when a meander  
 617 becomes very curved and the two concave banks at the extremity of the meander  
 618 becomes very close. The meander cutoff occurs when the neck of land between the  
 619 two concave banks is eroded due to the channel migration or due to strong current  
 620 during a flooding event. The meander is then abandoned and a shortcut in the channel  
 621 path is created where two concave banks are connected (Fig. 19).

622 In the proposed approach, this process is taken into account during the lateral  
 623 channel migration by detecting the self-intersections in the control point net of the  
 624 top surface of the channel.

625 [Fig. 19 about here.]

### 626 Segment intersection

627 Consider two non-parallel segments belonging, for instance, to the control mesh of  
 628 a channel top surface. Their intersection can be computed by determining two scalar  
 629 values  $a$  and  $b$  such that

$$\begin{array}{c}
 \begin{array}{ccc}
 & \text{pt2} + \vec{\text{vect2}} & \text{pt1} + \vec{\text{vect1}} \\
 & \nearrow & \nearrow \\
 \mathbf{p}_1 + a \mathbf{v}_1 = \mathbf{p}_2 + b \mathbf{v}_2 & \text{pt2} + b \vec{\text{vect2}} & \text{pt1} + a \vec{\text{vect1}} \\
 & \nwarrow & \nwarrow \\
 & \text{pt1} & \text{pt2}
 \end{array}
 \end{array}
 \quad (8)$$

630 where  $\mathbf{p}_1$  is the origin of the first segment,  $\mathbf{p}_2$  the origin of the second segment,  
 631 and  $\mathbf{v}_1$  and  $\mathbf{v}_2$  the vectors corresponding to the segments.

632 Taking the cross product of (8) with  $\mathbf{v}_1$  and  $\mathbf{v}_2$ , respectively, the following equa-  
 633 tion comes for  $a$  and  $b$ :

$$\begin{cases}
 a (\mathbf{v}_1 \times \mathbf{v}_2) = (\mathbf{p}_2 - \mathbf{p}_1) \times \mathbf{v}_2 \\
 b (\mathbf{v}_2 \times \mathbf{v}_1) = (\mathbf{p}_1 - \mathbf{p}_2) \times \mathbf{v}_1
 \end{cases}
 \quad (9)$$

634 If  $0 \leq a \leq 1$  and  $0 \leq b \leq 1$ , the two segments intersect and the coordinates of the  
 635 intersection points are given by  $\mathbf{p}_{inter} = \mathbf{p}_1 + a \mathbf{v}_1$ .

### 636 Construction of an oxbow lake

637 [Fig. 20 about here.]

638 The construction of an oxbow lake from a NURBS channel is divided in five  
 639 steps:

- 640 (i) Detection of the self-intersection for each side of the channel top surface (Fig. 20(a)).  
 641 The index of the channel sections behind and ahead of the intersecting segments  
 642 are memorized.

- 643 (ii) Sorting and reduction of the number of intersections. This operation may be  
644 needed to keep only one intersection, see below.
- 645 (iii) Increasing knot multiplicity at the parametric coordinate corresponding to the  
646 projection of the intersection point on the NURBS. This operation is used to de-  
647 crease the continuity of the NURBS while preserving its shape.
- 648 (iv) Selection of the sections before and after the intersection point (Fig. 20(b)).
- 649 (v) Lateral closure of the oxbow lake sections and connection of the cutoff sections  
650 to maintain channel continuity (Fig. 20(c))

651 [Fig. 21 about here.]

652 The proposed intersection sorting is essential to obtain consistent final geometry.  
653 For each intersection, a couple of channel section indices is determined. Their number  
654 has to be reduced so that only one intersection by meander remains. Four possible  
655 configurations have been determined. If there is only one intersection in the meander,  
656 then it is directly stored in the final intersection list (Fig. 21(a)). If two sections are  
657 included into another one, only the largest one is kept in the final list (Fig. 21(b)). If  
658 the first element of a couple of sections linked with a self-intersection is included in  
659 the space defined by another couple, the second couple of intersections is kept in the  
660 final list of intersections (Fig. 21(c)). If the second element of a couple of sections  
661 linked with a self-intersection is included in the space defined by another couple, the  
662 first couple of intersections is kept in the final list of intersections (Fig. 21(d)).

663 Once the final intersection list has been determined, the control points between  
664 two sections corresponding to an intersection are removed from the channel (Fig. 20(c)).  
665 The result of the channel lateral migration process associated with the construction  
666 of oxbow lakes is shown on Fig. 22.

667 [Fig. 22 about here.]

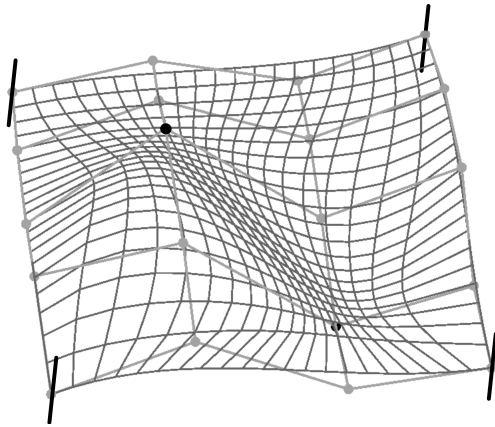


**Fig. 1** Bi-cubic NURBS surface with weight  $w = 10$  at the black points and  $w = 1$  at the grey points. The dark grey lines representing iso-parametric evaluations of the surface are particularly attracted around these two points

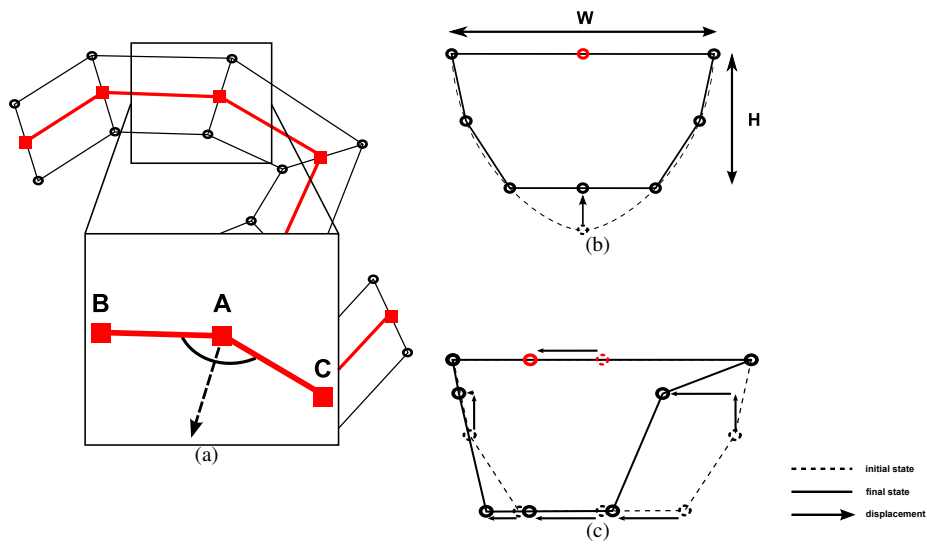


**Fig. 2** Construction steps for a channel section. (a) Sections are constructed for each point of the backbone (in red) and are aligned on the bisector between two consecutive segments. (b) The points of the section are placed along a quadratic function defined from the width  $W$  and height  $H$  of the channel. (c) Points are translated to obtain the desired asymmetry

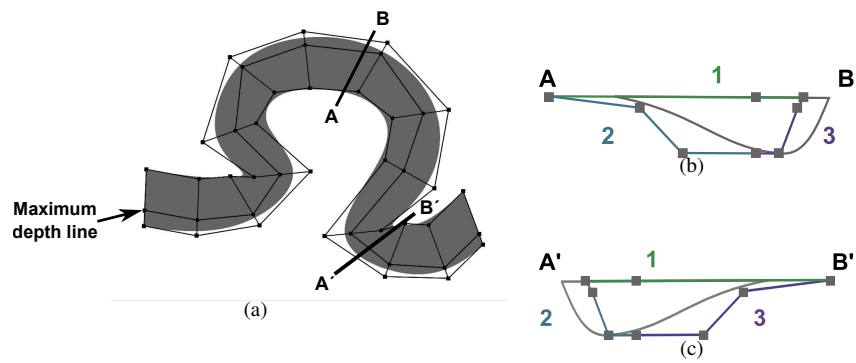


**Fig. 3** Model of an asymmetric channel based on NURBS surfaces (modified from Ruiu et al (2014)) (a) Top view of the channel (the control point net is represented by black lines). (b) Section view of the asymmetric channel in a positive channel curvature (a different color is used for each surface control point net). (c) Section view of the channel with an inverse asymmetry corresponding to a negative channel curvature

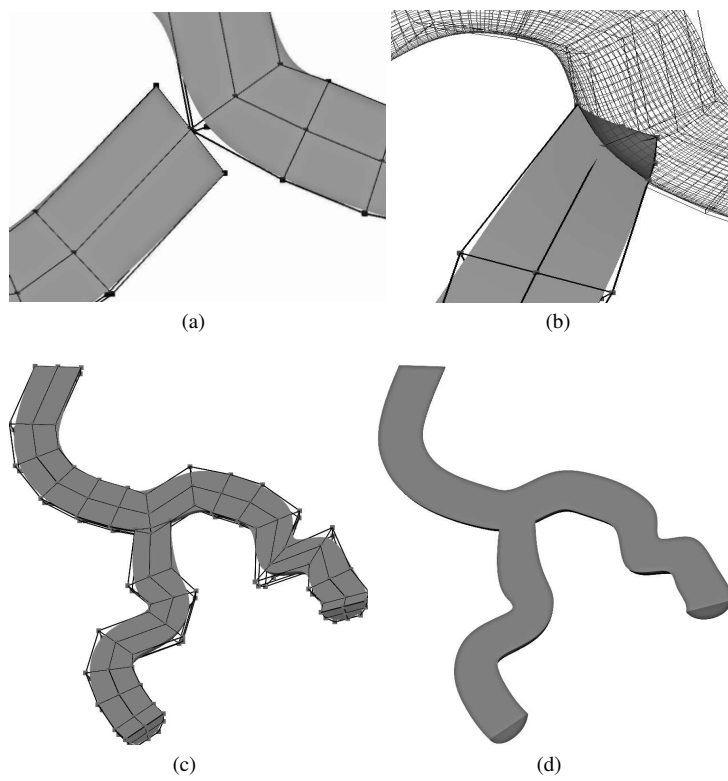


**Fig. 4** Process to branch to channels. (a) Extremity of the channel to link is aligned on the main channel. (b) This extremity is projected on the main channel. (c) Result with the control points. (d) Result with the channels only



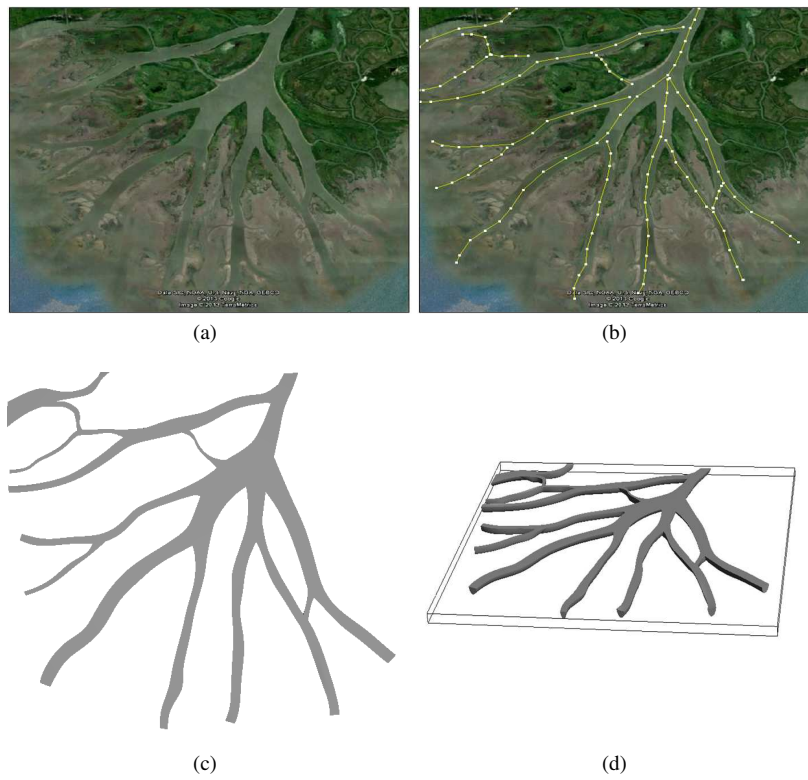


**Fig. 5** Application of the channel branching Process: manual three-dimensional interpretation (with an arbitrary thickness value) of thirteen channels on a satellite image of Atchafalaya Delta (Google Earth, October,29 2012). (a) Original image. (b) Pickings of channels (1 line by channel). (c) Result in top view. (d) Result in top lateral view

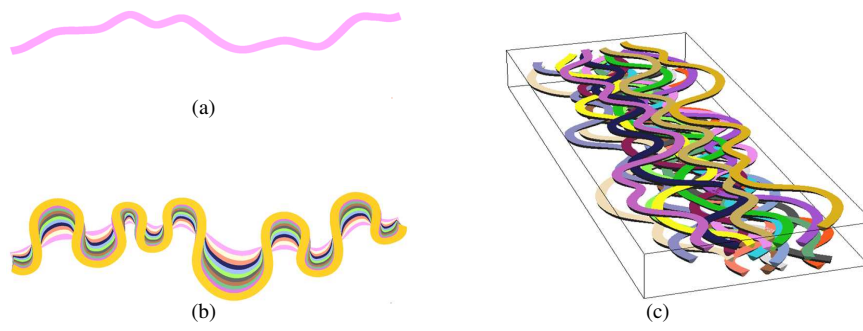


**Fig. 6** Construction of ten channels using a stochastically generated backbone. (a) The channel path is generated using an unconditional sequential Gaussian simulation. (b) Lateral migration steps of a channel. (c) Simulation of ten channels

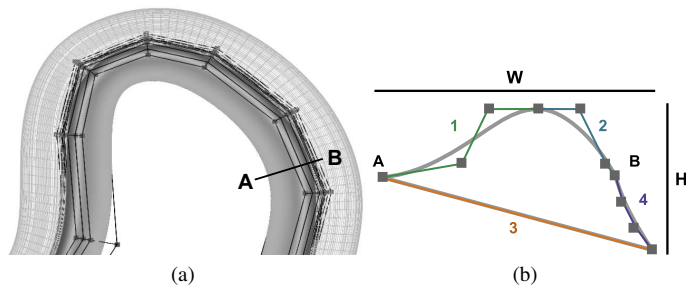


**Fig. 7** Modeling of a levee using four NURBS surfaces placed according to the width  $W$  and height  $H$  of the levee. Black lines represent the control net and grey points the control points. (a) Top view of the levee with its related channel (in wireframe mode). (b) Section view of the levee

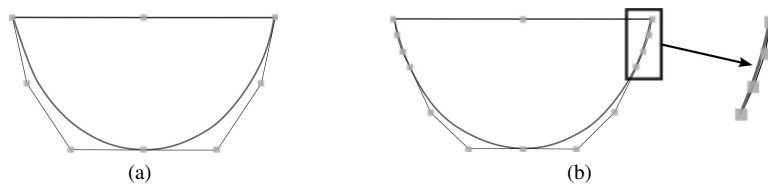


**Fig. 8** Extraction of a portion of parametric surface.(a) Initial state (b)Adding knots lead to add control points on the channel. Knots are added at the desired parametric coordinate in order to maintain the shape of the parametric surface. The knot is added to have a multiplicity equal the degree of the NURBS plus one in order to obtain  $C_0$  surface at this point and to ensure the surface goes through the control points

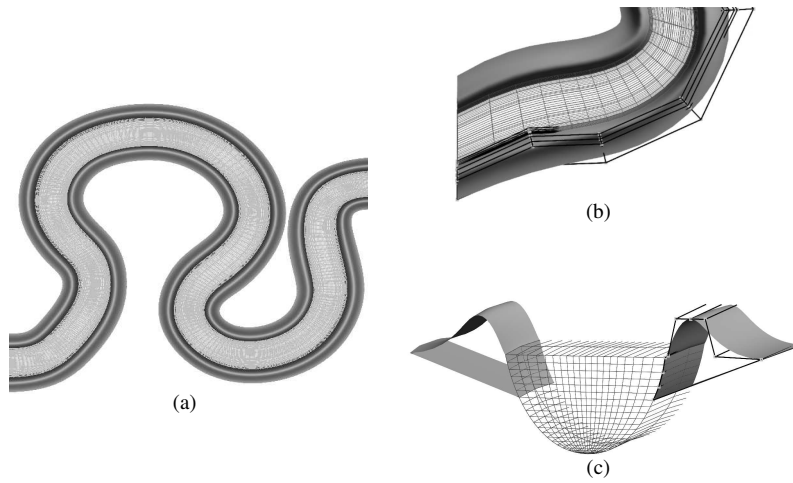


**Fig. 9** Levees are constructed in association to a channel. (a) Top view of levees associated with a channel. (b) Zoom on the top view (Channel in wireframe mode). (c) Lateral section of the channel and its levees showing the coherency in depth between the forms

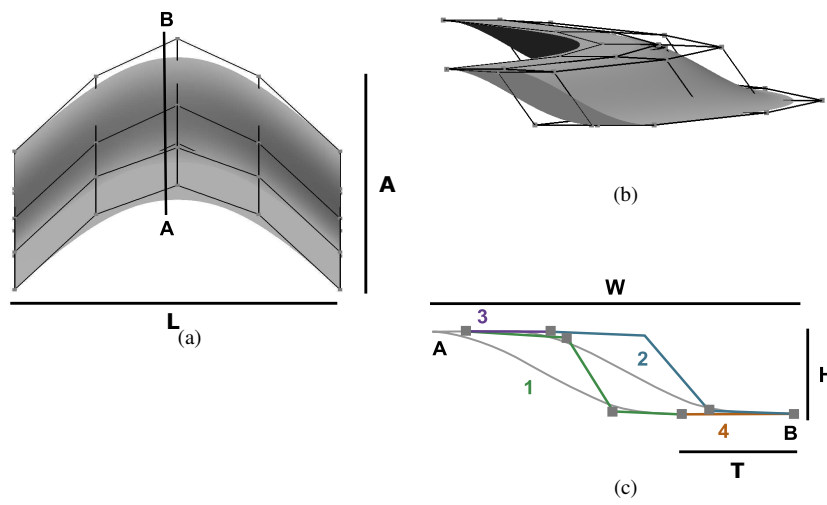


**Fig. 10** Modeling of a clinoform using six NURBS surfaces from width  $W$ , height  $H$ , thickness  $T$ , length  $L$  of the clinoform and the amplitude  $A$  of the channel which has formed the clinoform. Black lines are the control point net and the grey points are control points. (a) Top view of the clinoform. (b) Side view of the clinoform. (c) Section view of the clinoform

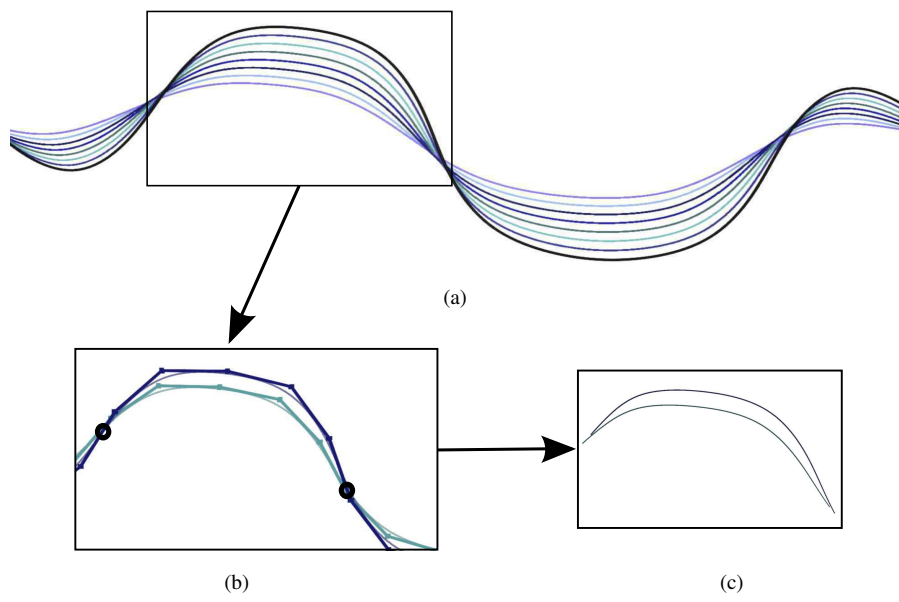


**Fig. 11** Extraction of a clinoform from a channel growing process. The channels are presented using their maximum depth lines. (a) A channel with its growing steps (in black final state and in color the others). (b) The intersections between the control net of these surfaces are computed. (c) Surface parts between the intersection points are extracted

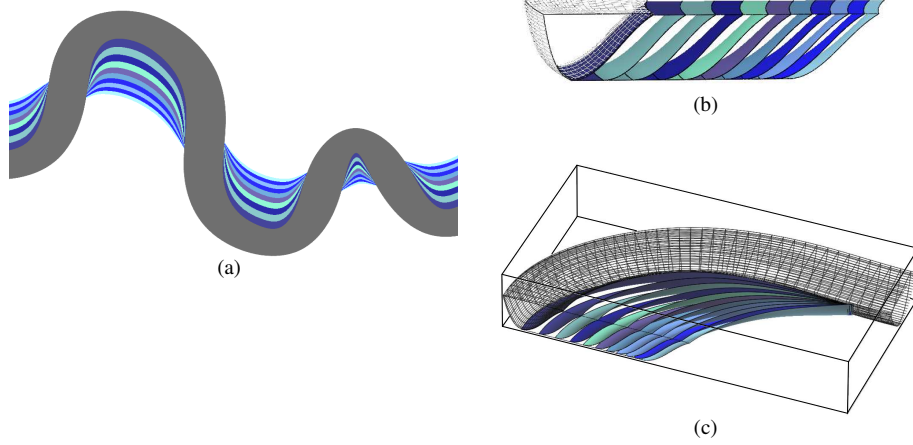


**Fig. 12** Clinoforms are extracted from simulated channel growth. (a) Clinoforms in top view associated with a channel. (b) Slab view of the clinoform succession (c) Cut off view of the channel and its clinoforms showing the coherency between the different forms in three-dimensional



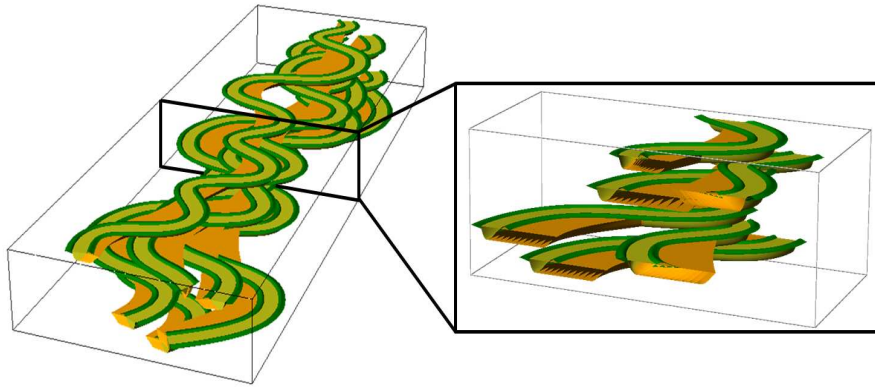


**Fig. 13** Realization of a fluvial deposit environment presenting four channels (in yellow) with their associated point bars (in orange) and levees (in green)

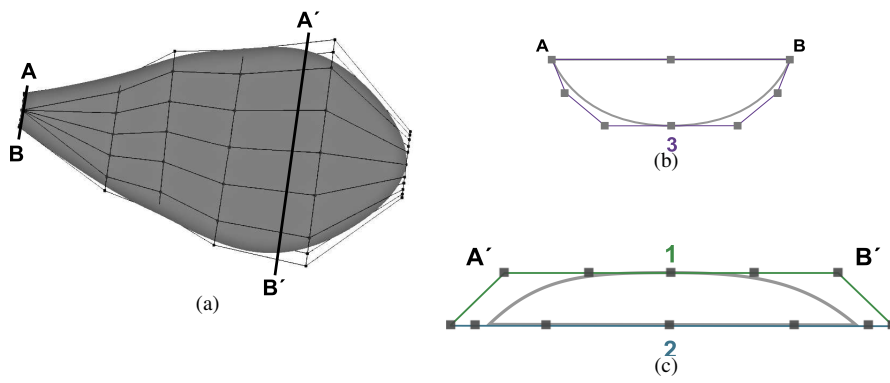


**Fig. 14** Modeling of a lobe shape using three NURBS surfaces. Black lines are the control point net and the grey points are control points. (a) Top view of the lobe (b) Channel shaped section connecting the lobe to the extremity of a channel. (c) Lens shaped section

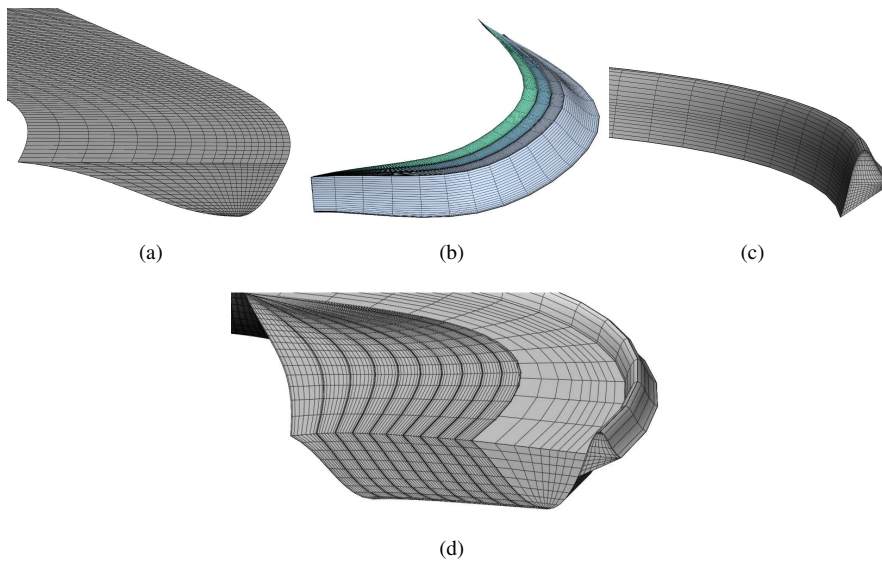


**Fig. 15** Hexahedral grids constructed from NURBS based boundary representations using different types of filling methods (a) Grid constructed from a channel. (b) Grids constructed from clinoforms (c) Grid constructed from a levee. (d) Relations between these different grids

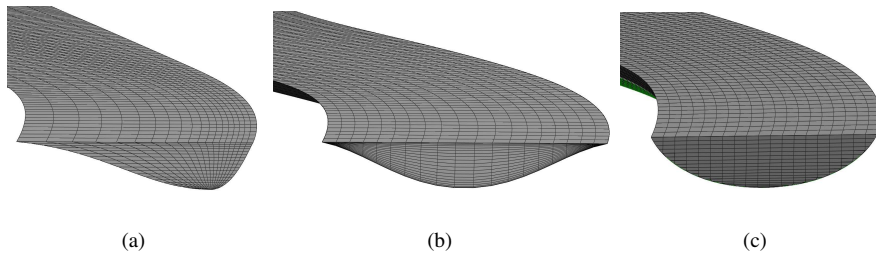


**Fig. 16** Hexahedral grids constructed from NURBS boundary representations using different types of filling methods (Reineck and Singh, 1980) (a) Prograding channel. (b) Divergent channel. (c) Aggrading channel

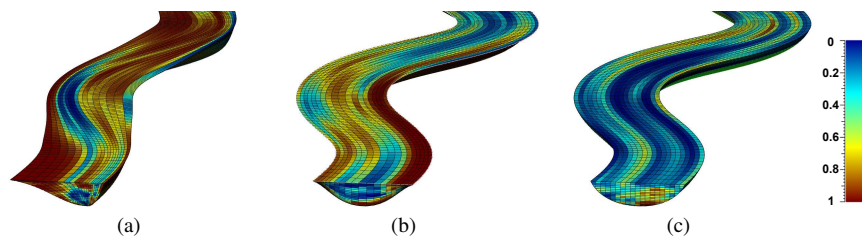


**Fig. 17** Porosity values simulated using channel grids (a) Prograding channel. (b) Divergent channel. (c) Aggrading channel

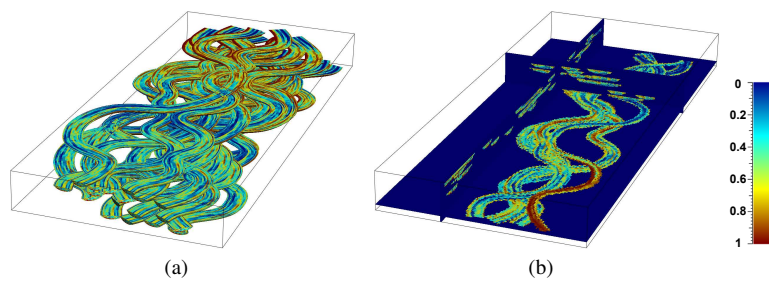


**Fig. 18** Upscaling of divergent channel porosity values simulated using unconditional SGS (in this case the same stochastic seed has been used for each channel porosity simulation) (a) Divergent channel grids to upscale (b) Upscaling result

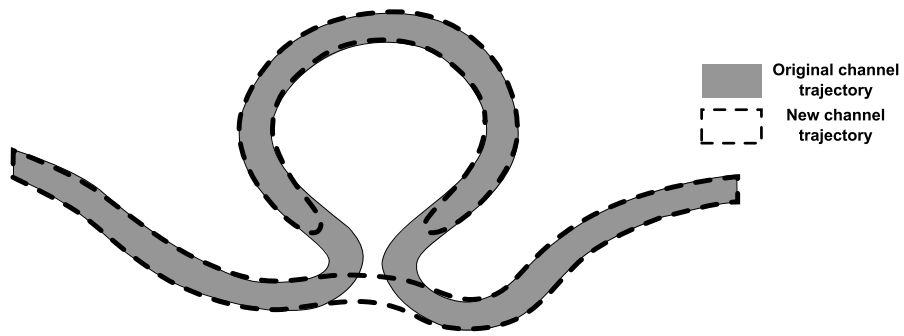


**Fig. 19** Principle of the formation of an oxbow lake during the lateral migration of a meander

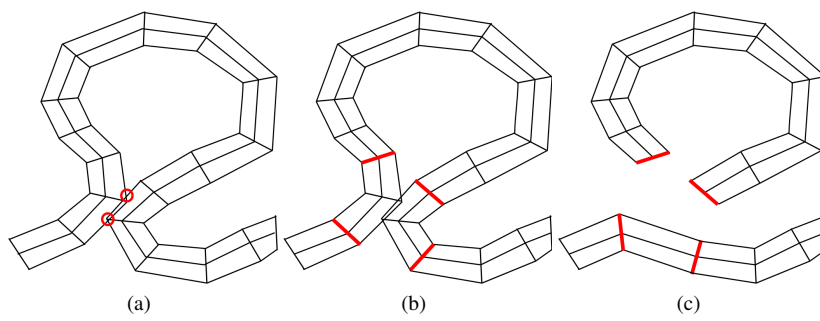


**Fig. 20** Construction of an oxbow. During the process of a channel lateral migration, self intersections can occur and are associated with the formation of an oxbow lake. (a) Self intersections are detected (Red points). (b) Sections before and after the self intersection are detected (red lines). (c) Control point between sections are detected and suppressed to form the oxbow lake and the new channel path



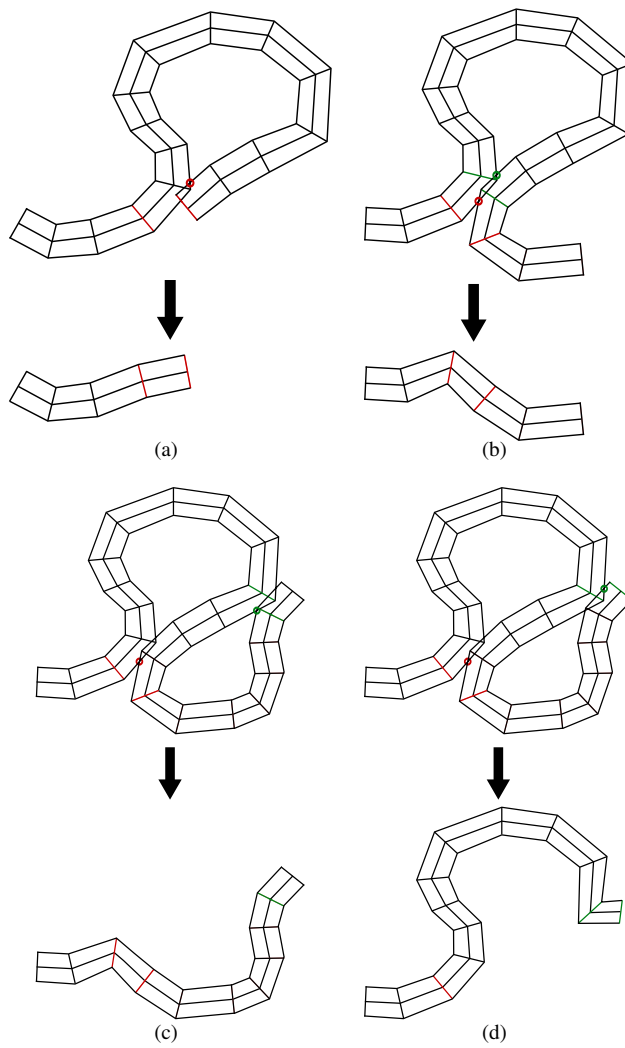


**Fig. 21** Sorting of the different cases of self-intersections during the NURBS channel migration. (a) Unique intersection. (b) Sections associated with an intersection are included between the sections corresponding to another intersection. (c) The first intersection associated with an intersection is included between the sections corresponding to another intersections. (d) The second intersection associated with an intersection is included between the sections corresponding to another intersections



**Fig. 22** Result of the oxbow lake formation during the channel lateral migration

Sedimentary order	Fluvial architectural elements	Specifics characteristics
1 <sup>st</sup> order	microforms (ripples)	Centimeter scale undulations with little or no apparent erosion.
2 <sup>nd</sup> order	mesoforms (dunes)	Large meter scale ripple with little or no apparent erosion.
<b>3<sup>rd</sup> order</b>	macroforms of growth increment (clinoform formed by the lateral accretion increment in channel)	Dipping depends of width depth ratio of the channel, usually up to 15° in the direction of accretion.
<b>4<sup>th</sup> order</b>	macroforms (point bars, levee, crevasse splay)	Variable geometries depending of the nature of the architectural element. Extension can be between few meters to few kilometres.
<b>5<sup>th</sup> order</b>	channel	Defined by width, length, depth, width/depth ratio with a concave up basal surface.

**Table 1** Hierarchy of fluvial architectural elements, after Miall (1996). The sedimentary orders addressed in this paper are in bold